Journal of Structural Geology 34 (2012) 20–29

Contents lists available at SciVerse ScienceDirect

Journal of Structural Geology

journal homepage: www.elsevier.com/locate/jsg

Microstructure and origin of faults in siliceous mudstone at the Horonobe Underground Research Laboratory site, Japan

Eiichi Ishii

Horonobe Underground Research Unit, Japan Atomic Energy Agency, Hokushin 432-2, Horonobe-cho, Hokkaido 098-3224, Japan

ARTICLE INFO

Article history:
Received 21 February 2011
Received in revised form
12 October 2011
Accepted 1 November 2011
Available online 9 November 2011

Keywords:
Microstructure
Fault
Shear band
Mudstone

ABSTRACT

Fault-related microstructures and fault orientations in siliceous mudstone were studied at the Horonobe Underground Research Laboratory site in Japan. Thin dark bands define a weak foliation that exhibits compactional cataclastic fabrics in thin section. These fabrics were observed both along the faults and beyond the fault tips, in outcrop and in drill core. Most of the bands are so thin that it was not possible to measure their thickness in thin section. However, scanning electron microscope images of fault surfaces revealed evidence of chemical compaction within the bands. Millimeter-scale displacements occur along similar dark bands in diatomaceous mudstone, which overlies the siliceous mudstone. In all boreholes, the dominant orientation of unfolded faults is WNW–ESE strike and a near-vertical dip. These observations suggest that the faults formed along compactional shear bands that in turn nucleated under ductile or brittle–ductile conditions. The development of compactional shear bands preceded fault formation, occurring just prior to folding, in response to E–W compression related to the eastward migration of the Amurian plate.

1. Introduction

The low permeability and high sorption capacity of mudstone makes it an important natural barrier in radioactive-waste-disposal facilities (Mazurek et al., 2008, 2011). However, when either shear stress—induced by tectonic forces—or nonhydrostatic stress exceeds the rock shear strength, brittle or ductile deformation may occur depending on the brittleness of the mudstone (Bjørlykke and Høeg, 1997; Nygård et al., 2006). If a mudstone is subjected to ductile deformation, it is unlikely that mudstone permeability will increase significantly because ductile deformation is only weakly or non-dilatant (Dehandschutter et al., 2004, 2005; Ishii et al., 2011a). However, if a mudstone is subjected to brittle deformation, the resulting structures may significantly increase the permeability because brittle deformation is strongly dilatant (Dehandschutter et al., 2004, 2005; Ishii et al., 2011a). Thus, an understanding of the relationship between brittleness and deformation behavior in mudstone is crucial for assessing the long-term efficacy of mudstone as a barrier in disposal repositories for radioactive waste.

Natural deformation structures observed in the field may record previous episodes of brittle or ductile deformation behavior, which can lead to an understanding of the relationship between brittleness and deformation behavior in a rock. When defined on the basis of specific rheological behavior (e.g., Dehandschutter et al., 2004, 2005; Ishii et al., 2011a), ductile deformation is characterized by weakly dilatant or non-dilatant behavior associated with strain hardening (in response to compaction). In contrast, brittle deformation is characterized by strongly dilatant behavior unrelated to strain hardening. So, for example, compactional shear bands, which are deformation bands (tabular discontinuities) often observed in sandstones (e.g., Aydin et al., 2006; Fossen et al., 2007), can be indicators of ductile deformation (Ishii et al., 2011a) because they are associated with physical/chemical compaction (strain hardening) processes such as alignment/rotation/disaggregation, cataclasis/comminution, and the pressure solution of constituent materials (Aydin et al., 2006; Fossen et al., 2007; Schultz and Fossen, 2008; Fossen, 2010). On the other hand, joints (opening mode fractures) are indicators of brittle deformation because they form by dilatant deformation that is unrelated to strain hardening (Ishii et al., 2011a). However, faults (slip surfaces) alone are insufficient indicators of ductile or brittle deformation because faults are not known to nucleate and self-propagate (Crider and Peacock, 2004; Aydin et al., 2006). Faults are generally associated with other deformation structures such as compactional shear bands or joints. When faults originate from compactional shear bands, fault initiation is thought to occur in a ductile regime through strain hardening (the formation of compactional shear bands) followed by strain softening (the formation of faults) (e.g., Schultz and Siddharthan, 2005; Torabi and

E-mail addresses: eishii33@yahoo.co.jp, eishii@numo.or.jp.

0191-8141/$ – see front matter © 2011 Elsevier Ltd. All rights reserved.
doi:10.1016/j.jsg.2011.11.001

Berg, 2011). On the other hand, when faults originate from joints, the ensuing faults are sheared/faulted joints (e.g., Wilkins et al., 2001; Myers and Aydin, 2004) that developed during brittle deformation.

Detailed observations of fault microstructures will reveal the mechanism of fault nucleation; i.e., brittle or ductile deformation. In particular, where faults nucleate from ductile deformation processes, detailed microstructural characterization of the fault reveals evidence of strain hardening (compactional deformation) during fault nucleation. For example, the development of faults in sandstones is well understood, as is their detailed textural evolution, where numerous faults originate as compactional shear bands with porosity-reducing structures (e.g., Aydin et al., 2006; Fossen et al., 2007). Vannucchi et al. (2003) studied faults in scaly clay using a scanning electron microscope (SEM) to observe the fault-related microstructures of faults, revealing that the faults originated from localized zones of aligned clay minerals. However, few studies have examined the microstructure of faults with a view to understanding the origin of faults in mudstone (Dehandschutter et al., 2004, 2005). In siliceous rocks, shear and tensile deformation mechanisms of fault formation have been studied (e.g., Gross, 1995; Wilkins et al., 2001; Ishii et al., 2010). However, the rheologies and microstructures of faults developing from shear deformation have received little attention.

Abundant faults occur in siliceous mudstone at the Horonobe Underground Research Laboratory (URL) site in Japan; their origin has not previously been identified. This study draws upon field descriptions, analyses of thin section, SEM observations of fault microstructures, and fault orientations in boreholes to determine the origin of faults developed in siliceous mudstone.

2. Geological background

The Horonobe URL site is located on the eastern margin of a Neogene to Quaternary sedimentary basin on the western side of northern Hokkaido, in a Quaternary, active foreland fold-and-thrust belt near the boundary between the Okhotsk and Amurian plates (e.g., Yamamoto, 1979; Wei and Seno, 1998; Ikeda, 2002) (Fig. 1). The basin fill consists of the Wakkanai, Koetoi, Yuchi, and Sarabetsu formations, from bottom to top (Figs. 1 and 2).

The Wakkanai Formation, a Neogene siliceous mudstone, is poorly exposed at the Horonobe URL site. The siliceous mudstone, for the most part, is a single, massive, homogeneous lithofacies (Mitsui and Taguchi, 1977; Iijima and Tada, 1981; Hiraga and Ishii, 2008), though weakly developed bedding planes can be recognized by electrical micro-imaging in boreholes (Ishii et al., 2006). Mineralogically, siliceous mudstone consists of 40–50 wt.% silica (mainly

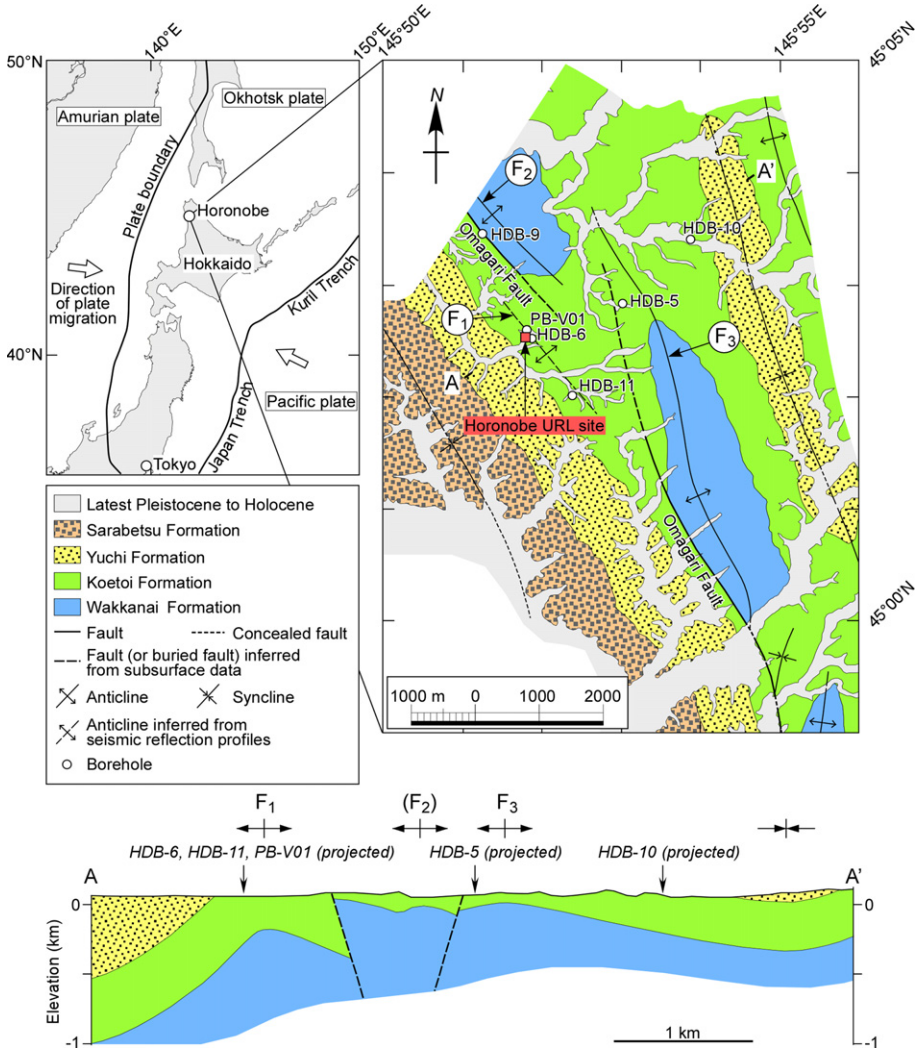

Fig. 1. Geological map and geological cross-section of the Horonobe area (after Ishii et al., 2008), showing the locations of boreholes and the Horonobe URL site. Plate boundaries and directions of plate movement shown in the inset map are from Wei and Seno (1998). F_1, F_2, and F_3 are specific fold hinges analyzed in this study.

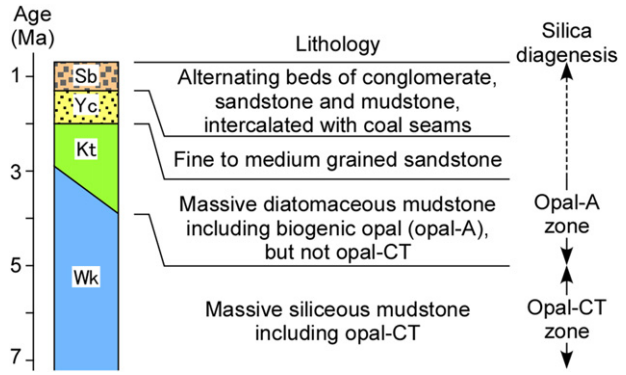

Fig. 2. Schematic columnar section of the Horonobe area (Ishii et al., 2010). Sb: Sarabetsu Formation; Yc: Yuchi Formation; Kt: Koetoi Formation; Wk: Wakkanai Formation.

opal-CT), 19–33 wt.% clay (10–18 wt.% smectite and 7–13 wt.% illite), quartz (9–13 wt.%), feldspar (7–13 wt.%), pyrite (0–4 wt.%), and carbonate (0–1 wt.%), based on normative calculations (Mazurek and Eggenberger, 2005; Hiraga and Ishii, 2008). The effective porosity is 30%–50% (Sanada et al., 2009). The siliceous mudstone formed from the induration of diatomaceous mudstone during progressive burial diagenesis of silica minerals, involving the dissolution of opal-A and the precipitation of opal-CT within pore spaces (Ishii et al., 2011b). A massive and relatively soft diatomaceous mudstone, the Koetoi Formation, overlies the siliceous mudstone. Mineralogically, the diatomaceous mudstone consists predominantly of opal-A (40–50 wt.%) and clay (17–25 wt.%, comprising 9–17 wt.% illite and 0–11 wt.% smectite) with lesser amounts of quartz (7–10 wt.%), feldspar (5–10 wt.%), pyrite (0–2 wt.%), and carbonate (0–2 wt.%), based on normative calculations (Mazurek and Eggenberger, 2005; Hiraga and Ishii, 2008). The effective porosity is 45–65% (Sanada et al., 2009). The lithological boundary between the two mudstones is a gradual, conformable transition.

Burial and subsidence of the Wakkanai, Koetoi and Yuchi formations occurred during the Neogene–Quaternary. The siliceous mudstone was buried to a depth of more than 1 km at the time of maximum burial (Ishii et al., 2008; Kai and Maekawa, 2009). Subsequently, uplift and denudation started at about 1 Ma with the deposition of the Sarabetsu Formation, which followed flexural folding that began between 2.2 and 1.0 Ma in response to regional E–W compression (Ishii et al., 2008). Some anticline hinge lines (e.g., F_1, F_2, and F_3 in Fig. 1) developed with NW–SE to NNW–SSE trends, plunging gently to the northwest or southeast.

In the folded siliceous mudstone, abundant predominantly strike-slip faults crosscut bedding planes at a high angle, and bedding-parallel faults are observed in outcrop and in drill core (Ishii and Fukushima, 2006; Ishii et al., 2010). The strike-slip faults with fault breccias occur at shallower depths in the siliceous mudstone and are associated with numerous splay joints. Such faults are highly permeable structures (Ishii et al., 2010) whose origin and nucleation age are poorly constrained.

This study focuses on the faults that crosscut bedding planes at a high angle, which are simply called “the faults” or “faults” herein. A “fault” is defined as a slip surface with slickensides, associated with fault rocks, slickenlines, and/or slickensteps.

3. Observations and results

3.1. Microstructures

Dark bands are closely associated with the faults in siliceous mudstone outcrops. The dark bands are observable at and beyond fault tips near faults with fault breccias (Fig. 3a). Although dark bands are too thin to measure in the field, they are recognized by their dark color, which contrasts with the surrounding siliceous mudstone. The bands can be traced over lengths of less than 10 cm. Dark bands are also observed at and beyond isolated faults that lack fault breccias (Fig. 3b and c). The fault surfaces are identifiable as dark planes in outcrop and in drill core (Fig. 3d: the dark planes are odorless and are unrelated to hydrocarbons), and were not observed on joint surfaces. A lack of marker horizons means it is not possible to observe displacement along bands in siliceous mudstone. However, similar dark bands (somewhat thicker at 0.1–5.0 mm) occur in diatomaceous mudstone (Fig. 3e), which preserves numerous trace fossils that serve as markers and that record millimeter-scale displacements (Fig. 3f). The fault surfaces in the diatomaceous mudstone are similarly identifiable as dark planes (Fig. 3g).

In thin section, a weak foliation oriented sub-parallel to dark bands in siliceous mudstone is defined by the preferred orientation of tabular crystals (e.g., feldspar), very fine-grained minerals (possibly clay minerals such as illite), and small, black, fine-grained cataclasite bands (Fig. 4a). Such a foliation is not observed in the surrounding matrix. Although quartz and feldspar cataclasis was not observed within dark bands, the boundaries between bands and the surrounding matrix are sharp (Fig. 4a). Dark bands were also observed along fault planes and are similarly associated with a weak foliation developed sub-parallel to faults (Fig. 4b). Boundaries between bands and the matrix are sharper than those shown in Fig. 4a. In many cases, it is not possible to measure band thicknesses, even in thin section (Fig. 4c). The development of a weak foliation similar to that described above (e.g., Fig. 4a) was also observed for dark bands in diatomaceous mudstone, though boundaries between bands and the matrix are more diffuse than those observed along fault planes and within siliceous mudstone (Fig. 4d).

High-resolution SEM observations of fault surfaces show that very thin dark bands along faults have compactional textures. Silica-dominant gelatinous films occur across fault surfaces (Fig. 5a). It is difficult to discern individual grains within the film. However, where grains can be differentiated, they are typically platy (both silica and clay particles), and are preferentially aligned parallel to the fault surface. Grain boundaries are diffuse and for the most part appear to fuse together, resulting in continuous silica films across fault surfaces. Although opal-CT lepispheres (authigenic silica) were not found at fault surfaces, they were observed as partly comminuted precipitates within pore spaces in the surrounding matrices (Fig. 5b). Similar textures were also observed along fault surfaces in diatomaceous mudstone (Fig. 5c), though the silica phase was different. Diatomaceous fragments are rare upon fault surfaces but are common in the surrounding matrix (Fig. 5c and d).

3.2. Orientation

The orientations of faults in boreholes were determined by making detailed correlations of drill core data with acoustic imagery data obtained with the borehole televiewer survey (BHTV) in HDB-6, HDB-9, HDB-10, HDB-11, and PB-V01, or the resistivity image data obtained with electrical micro-imaging (EMI) in HDB-5. Bedding plane orientations were determined by EMI, though the orientations in PB-V01, where EMI was not conducted, are taken to be the same as those in the neighboring borehole HDB-6 (Fig. 1).

Table 1 lists the orientations of bedding planes and faults, in boreholes. Fig. 6a–f shows poles to fault planes and bedding planes in boreholes, as well as poles to bedding faults, on lower hemisphere equal-area projections.

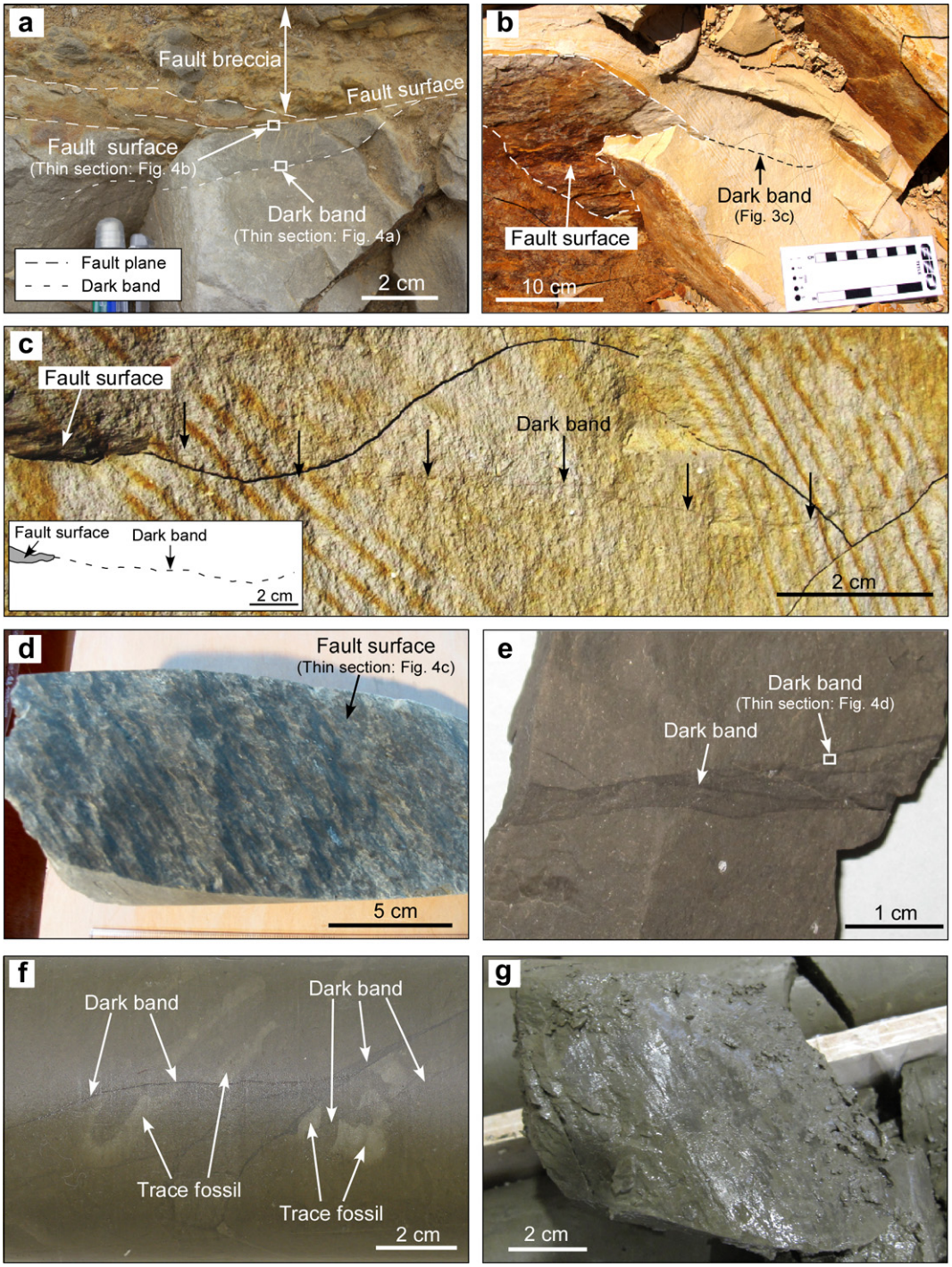

Fig. 3. Photographs of fault-related discontinuities. (a) Thin dark band observed near a fault with fault breccia in siliceous mudstone. The length of the dark band is about 10 cm. (b) Thin dark band in siliceous mudstone. (c) Close-up of the thin dark band in (b). The trace length of the dark band is about 10 cm. The dark band shows en-echelon-like or anastomosing geometries. The sketch at bottom left is an interpretation of the photograph. (d) Fault plane in drill core from the siliceous mudstone, showing dark planes. (e) Dark bands with measurable thicknesses in a hand specimen of diatomaceous mudstone. (f) Diatomaceous mudstone core, showing dark bands that cut trace fossils. (g) Fault plane in diatomaceous mudstone from drill core, showing dark planes.

Bedding plane orientations in HDB-6, HDB-9, HDB-11, and PB-V01, which are located along the western limb of folds 'F_1' and 'F_2' in Fig. 1, are very similar. These orientations differ a little from bedding plane orientations in HDB-5, which is located along the western limb of 'F_3' in Fig. 1. The bedding plane orientations in HDB-10, which is located along the eastern limb of 'F_3' in Fig. 1, are significantly different from those in the other boreholes (Table 1; Fig. 6a–f).

The major fault orientations in HDB-6, HDB-9, HDB-11, and PB-V01 are similar, and have lower dip angles than those in HDB-5 (Table 1; Fig. 6a–f). The major fault orientations in HDB-10 differ significantly from those within the other boreholes (Table 1; Fig. 6a–f). Minor fault orientations were also observed for some boreholes (Table 1; Fig. 6c–f).

Fig. 6g–i shows the unfolded orientations of features depicted in Fig. 6a–f; for unfolded geometries, bedding planes were rotated to

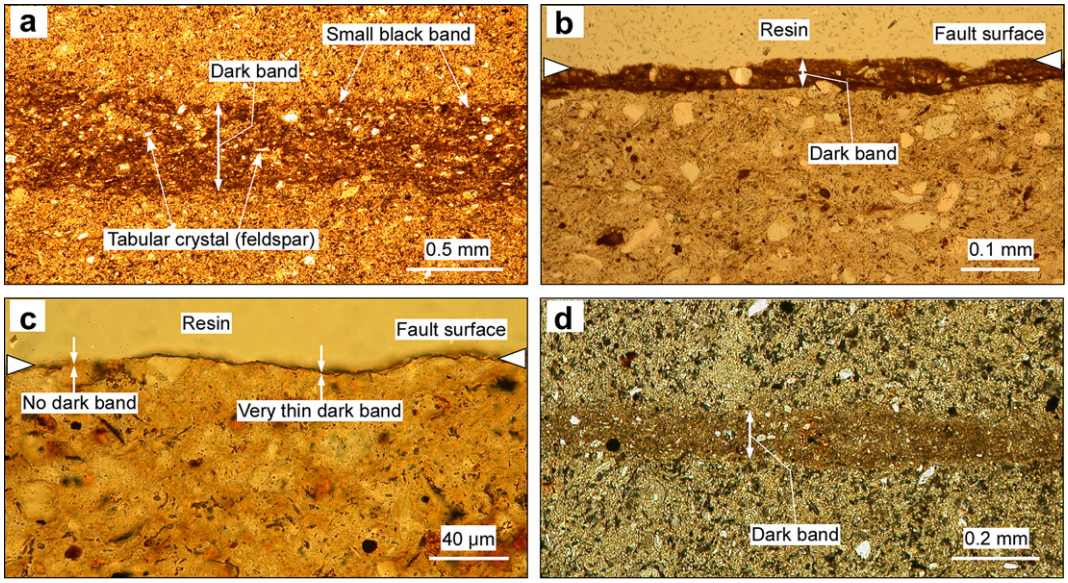

Fig. 4. Thin section photomicrographs of discontinuities (plane polarized light). (a) Dark band shown in Fig. 3a. Band thickness is about 0.5 mm. A weak, internal foliation is characterized by the preferred orientation of tabular crystals including feldspar and, possibly, by clay minerals such as illite. Small black bands indicating cataclasis are oriented sub-parallel to the dark band. This foliation is not present in the surrounding matrix. The boundary between the dark band and the matrix is sharp. Quartz and feldspar in the dark band are not fractured. (b) Dark band observed along the fault plane shown in Fig. 3a. Band thickness is about 0.05 mm. Band color is darker than in (a) and a weak foliation is oriented sub-parallel to the fault plane. The boundary between the dark band and the matrix is very sharp. Quartz and feldspar in the dark band are not fractured. (c) Very thin dark bands along the fault plane shown in Fig. 3d. At this scale, thicknesses were not measurable and it is possible that the bands are discontinuous along the fault plane. (d) Dark band shown in Fig. 3e. A weak internal foliation occurs sub-parallel to the dark band and is absent in the surrounding matrix. The boundary between the dark band and the matrix is diffuse. Quartz and feldspar in the band are not fractured.

the horizontal (see also Table 1). The rotation consists of the following process: first, a hold hinge was rotated to the horizontal if the hinge was plunging; second, the bedding plane was brought to the horizontal by rotating it around the horizontal fold hinge through an angle equal to the dip of the bed (following Silliphant et al., 2002). The unfolded major fault orientations in all boreholes are similar, striking WNW–ESE with near-vertical dips (Table 1; Fig. 6g–i). The unfolded minor fault orientations varied among the boreholes (Table 1; Fig. 6i–l).

4. Discussion

4.1. Origin of the faults

Thin dark bands were observed along and near faults. Observations of thin sections revealed weak foliations with compactional/cataclastic fabrics. Most of the bands along faults are too thin to determine their thicknesses, even in thin section. SEM observations of fault surfaces revealed a surface-parallel alignment of platy particles, and the existence of silica films with fused silica textures in bands along faults. Although opal-CT lepispheres were not found on fault surfaces, they were observed in adjacent matrices, although partly comminuted. Similar dark bands occur in diatomaceous mudstone, where millimeter-scale displacements were observed along bands. These observations indicate that the dark bands are compactional shear bands resulting from physical and chemical compaction, including the preferential alignment of platy particles, the cataclasis and comminution of relatively fragile opal-CT lepispheres, and the fusing-together of highly soluble opal-CT crystallites (Brueckner et al., 1987) to form silica films, thereby supporting the interpretation of the dark bands as compactional shear bands. The cataclasis/comminution of opal-CT lepispheres by compactional shearing seems to have encouraged the fusing-together (possibly dissolution, dispersion, precipitation, contact healing, grain growth, etc.) of opal-CT crystallites; an understanding of the detailed fusing-together mechanism needs further data to enable an adequate interpretation and discussion.

The dark bands were also observed at and beyond fault tips, indicating that fault formation followed the formation of compactional shear bands. This is coherent in a rheological sense. Usually, in terms of rheology, fault formation and compactional shear band formation correspond to strain softening and strain hardening, respectively (Aydin and Johnson, 1978; Dehandschutter et al., 2005; Ishii et al., 2011a), and strain softening follows strain hardening (Schultz and Siddharthan, 2005; Torabi and Berg, 2011). This is consistent with the above observations.

The transition from compactional shear band formation to fault formation likely proceeded as follows (referring to the model of Ben-Zion and Sammis, 2003). First, compactional shear bands formed through strain hardening resulting from initial strain localization, and possibly following strain delocalization. Subsequently, additional strain produced weak fabrics/planes (e.g., surfaces of silica films or fine-grained cataclastic zones) oriented sub-parallel to the developing shear zone with strain localization. Eventually, with strain softening, fault surfaces nucleated along the developed fabrics/planes (Fig. 7). Although joints, which originated as compactional deformation structures, may grow into faults with subsequent shear movement (Zhao and Johnson, 1992; Eichhubl et al., 2009), fault surfaces with both dark planes and plumose structures were not observed; therefore, such a growth history is not appropriate in explaining the formation of faults observed in this study.

Thus, the faults analyzed in this study are considered to have formed along compactional shear bands that nucleated under ductile conditions by a deformation process involving the formation of compactional shear bands prior to the development of faults. However, the band thicknesses are very thin, indicated that strain hardening may not have been significant. In turn, this may suggest that the faults nucleated in the brittle–ductile transitional regime rather than within the ductile regime.

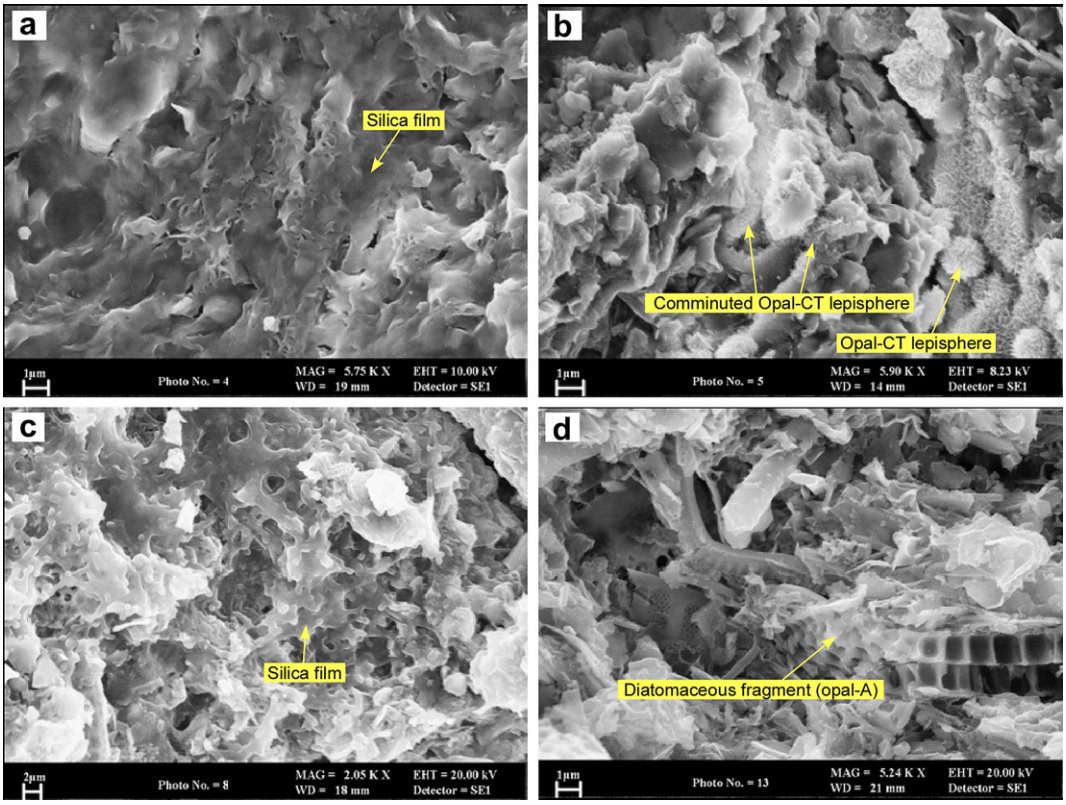

Fig. 5. High-resolution SEM images. (a) Fault surface in siliceous mudstone showing the surface-parallel alignment of platy particles and silica films. The films have fused silica textures. (b) Siliceous mudstone matrix adjacent to a fault surface, showing partially comminuted opal-CT lepispheres precipitated within pore spaces. (c) Fault surface in diatomaceous mudstone, showing the surface-parallel alignment of platy particles and silica films. The films have fused silica textures. (d) Diatomaceous mudstone matrix adjacent to the fault surface.

Deformation bands are known to develop in sandstone (e.g., Aydin et al., 2006; Fossen et al., 2007). However, the development of deformation bands in naturally deformed mudstone, as presented in this paper, is rare.

4.2. Nucleation age of the faults

The nucleation age of a fault is generally closely related to its orientation. For example, vertical fractures, regardless of bedding plane attitude in folded sedimentary rocks, likely formed after folding (Engelder et al., 2009). On the other hand, if fractures lack a preferred orientation in folded sedimentary rocks and are instead concentrated in a specific orientation in an unfolded state, these fractures likely formed in response to a regional tectonic stress before folding (Hennings et al., 2000; Silliphant et al., 2002; Guiton et al., 2003b; Mynatt et al., 2009).

In the present study, major fault orientations (in their unfolded state) in all boreholes are concentrated around a WNW–ESE strike, with nearly vertical dips (Fig. 6g–l). This is strong evidence that the faults formed before folding.

In addition, the concentration of fault orientations (Fig. 6) and the distribution of faults described by Ishii and Fukushima (2006) indicate that fault generation is due to tectonic deformation, considering the indicators used by Fossen (2010). The above WNW–ESE strike is oblique to the regional E–W directed compression (Ishii et al., 2008). Therefore, the faults began as strike-slip compactional shear bands just before folding was initiated (i.e., at around the maximum burial depth), in response to E–W compression due to the eastward migration of the Amurian plate (Fig. 1).

4.3. Relationship between fault origin and burial/uplift history

Deformation behavior is closely related to the history of burial and uplift of the host rocks (Ingram and Urai, 1999; Dehandschutter et al., 2004, 2005; Schultz and Fossen, 2008). For example, in the case of a normally consolidated sedimentary rock that is being

Table 1
Orientations (dip direction/dip) of bedding planes and faults in boreholes. F_1, F_2, and F_3 correspond to the fold hinges shown in Fig. 1.

Borehole	Bedding plane	Fault		Fault (unfolded)		Fold hinge used to rotate back to horizontal
		Major orientation	Minor orientation	Major orientation	Minor orientation	
HDB-5	265/35	015/65		29/81		335/13 (F_3)
HDB-6	225/35	010/53		17/83		140/3 (F_1)
HDB-9	230/40	030/50	170/57, 315/55	35/88	138/47, 341/61	140/0 (F_2)
HDB-10	055/40	217/57	160/50	37/85	180/68	335/8 (F_3)
HDB-11	230/40	005/55	280/45	15/86	331/34	140/0 (F_1)
PB-V01	225/35	000/45	269/43	13/73	316/28	140/3 (F_1)

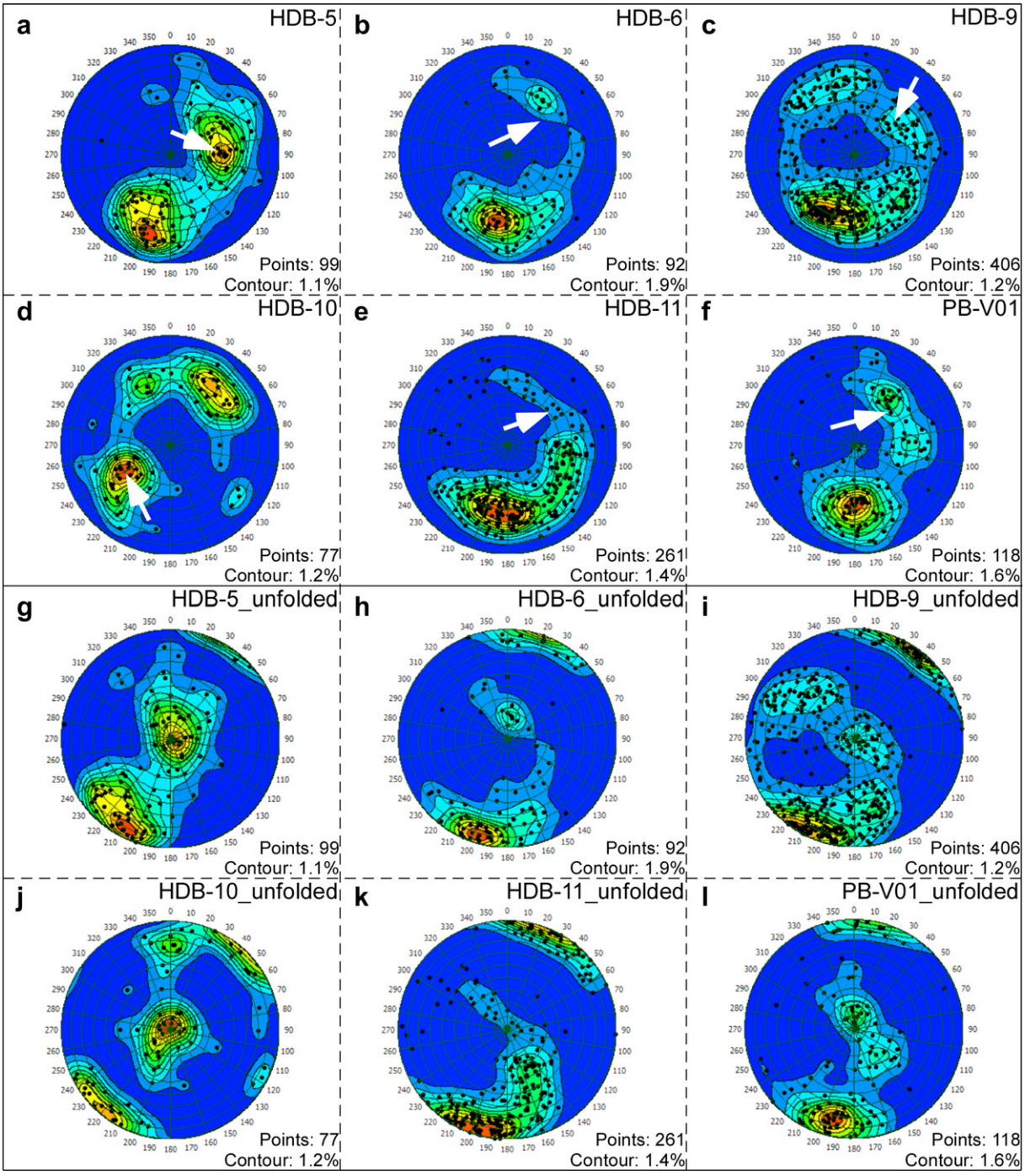

Fig. 6. Orientations of faults, bedding planes, and bedding faults in boreholes (a–f), and their unfolded orientations once the bedding planes have been rotated into the horizontal (g–l). The arrows point to bedding plane orientations. Note that major fault orientations in all boreholes are variable (a–f), while their unfolded orientations are largely consistent (g–l). Contours were made using the Fisher distribution (lower hemisphere equal-area projection).

progressively buried, ductile deformation generally occurs during shearing. In contrast, in the case of an overconsolidated sedimentary rock that may be subjected to uplift and denudation or to induration during mineral diagenesis, brittle deformation typically occurs during shearing.

The thinness of compactional shear bands along faults suggests that the faults nucleated in the brittle–ductile transitional regime rather than in the ductile regime, as mentioned above. However, the faults probably formed at or near the maximum burial depths, and the sedimentary rocks are estimated to have consolidated normally, in a ductile regime. On the other hand, the siliceous mudstone was indurated by burial silica diagenesis (Ishii et al., 2011b); such induration increases rock brittleness (Ingram and Urai, 1999). Therefore, the overconsolidated state created by silica diagenesis enabled the development of very thin compactional shear bands.

4.4. Growth history of the faults

The growth history of the faults is summarized as follows (Fig. 8). The strike-slip compactional shear bands and faults

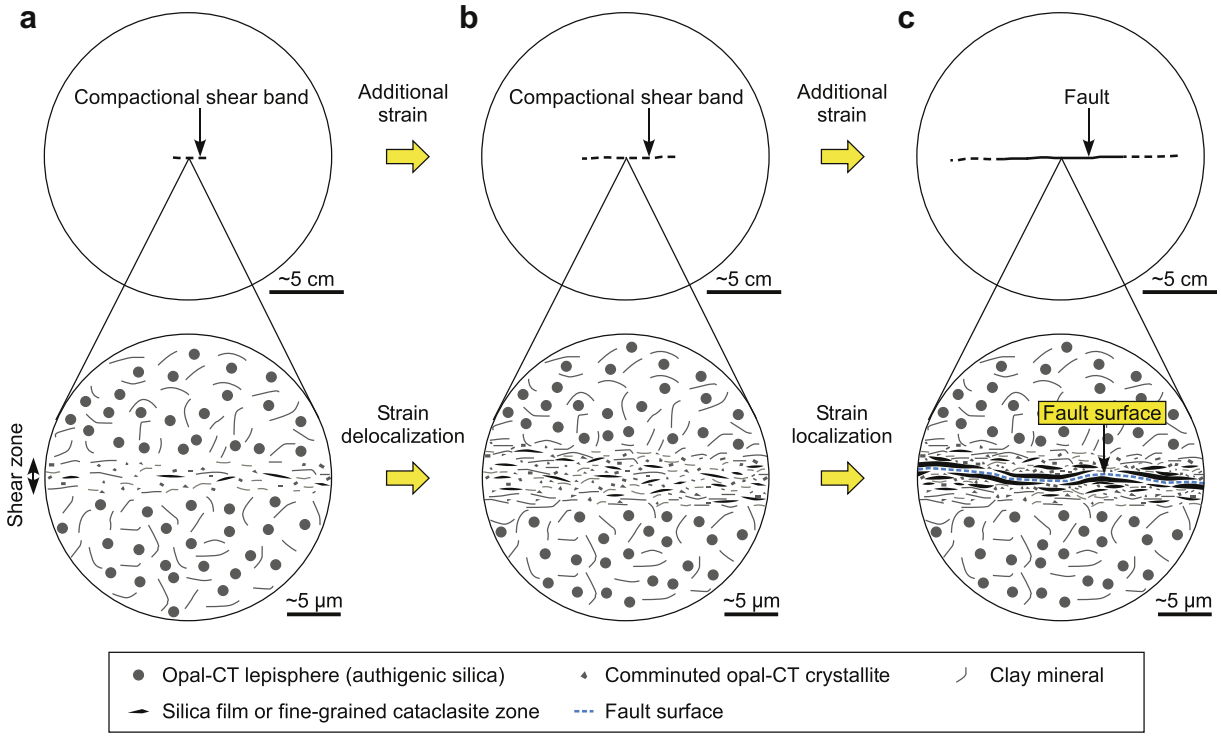

Fig. 7. Fault nucleation model for siliceous mudstone. (a) Nucleation of a compactional shear band by the preferred alignment of platy particles, the cataclasis/comminution of opal-CT lepispheres, and the fusing-together of opal-CT crystallites to form the silica films. (b) Band-parallel extension of the compactional shear band by additional strain, possibly with strain delocalization. (c) Nucleation of a fault surface along continuous and potentially weak fabrics/planes (e.g., surfaces of silica films or fine-grained cataclasite zones) oriented sub-parallel to the shear zone, due to additional strain with strain localization.

nucleated just before the initiation of folding in the brittle–ductile transitional or ductile regime, due to regional tectonic compression. At this time, if the faults were forming during deformation, propagation of the previously formed compactional shear bands may have facilitated linkages between the faults at extensional step-over fault positions, as deformation bands can easily link together in extensional step-over geometries (Okubo and Schultz, 2006). In the present study, extensional step-over fault geometries were often

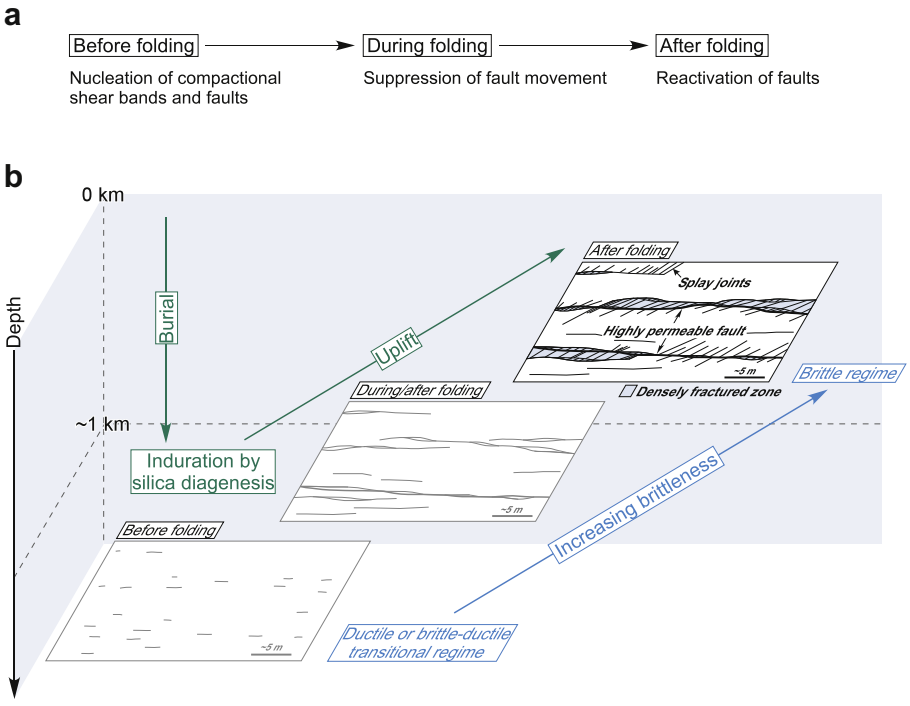

Fig. 8. (a) Temporal relationship between burial/uplift, folding, and fault movement. (b) Example of the growth history of a sinistral strike-slip fault. See the text for details.

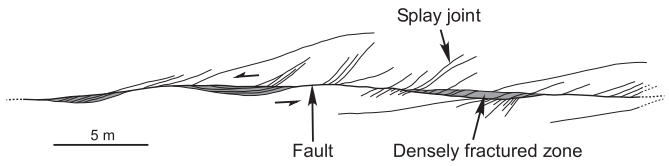

Fig. 9. Fault trace mapped on a horizontal outcrop (modified from Ishii and Fukushima, 2006). Numerous splay joints extend from the fault. Densely fractured zones occur at the locations of extensional step-over faults (Ishii et al., 2010).

observed in outcrop (Ishii and Fukushima, 2006; Fig. 9), some of which may have been inherited from compactional shear band linkage structures. On the other hand, although faults may be displaced by bedding faults that formed during folding (Ishii and Fukushima, 2006), the faults associated with fault breccias displace the bedding faults without exception, indicating they formed after folding (Iwatsuki et al., 2009; Ishii et al., 2010). Therefore, fault movement appears to have been suppressed during folding, probably due to the stress relief accommodated by the development of bedding faults (cf., Guiton et al., 2003a). Subsequent to folding, faults with fault breccias developed by preferential reactivation. However, just after folding, the siliceous mudstone had not yet experienced significant uplift (from hundreds of meters of depth) and the rocks were not especially brittle. Therefore, the faults probably continued to grow via the deformation process by which compactional shear band formation slightly preceded fault formation; this certainly seems reasonable for the period just after regional folding, because folding is commonly associated with ductile deformation rather than brittle deformation. As uplift and denudation progressed, the brittleness of the siliceous mudstone increased sufficiently to enable some faults to form at shallower depths in association with the development of numerous secondary splay joints. The faults are linked through the splay joints, resulting in a highly permeable fault network (Ishii et al., 2010). Nevertheless, at greater depths (greater than several hundreds of meters), few splay joints were observed in boreholes, and strong linkages between faults are absent (Ishii et al., 2010, 2011a).

5. Conclusions

Thin dark bands characterized by weak foliations and microscale compactional and cataclastic fabrics were observed in siliceous mudstone along faults and beyond fault tips in outcrop and in drill core. Most of the bands along faults are too thin to measure band thicknesses, even in thin section. SEM observations of fault surfaces revealed evidence of chemical compaction within bands along faults. Similar dark bands in diatomaceous mudstone (overlying the siliceous mudstone) show millimeter-scale displacements along bands. The major faults, in their unfolded state, are predominantly oriented around a WNW–ESE strike and are nearly vertical in all boreholes. These observations suggest that faults formed along compactional shear bands that nucleated in the ductile or brittle–ductile transitional regime. The formation of compactional shear bands preceded fault formation, just before the initiation of folding, in response to E–W compression due to the eastward migration of the Amurian plate. This type of information on the origin of faults is fundamental in understanding the relationship between brittleness and the deformation behavior of rock (Ishii et al., 2011a).

Acknowledgments

The British Geological Survey provided the SEM images in Fig. 5. A. E. Milodowski is thanked for providing the SEM observations. I would also like to extend my gratitude to T. Blenkinsop and B. Dehandschutter for their critical reviews of the manuscript, and to A. Stallard for editing the English and providing helpful suggestions.

References

Aydin, A., Johnson, A.M., 1978. Development of faults as zones of deformation bands and as slip surfaces in sandstone. Pure and Applied Geophysics 116, 931–942.
Aydin, A., Borjab, R.I., Eichhubl, P., 2006. Geological and mathematical framework for failure modes in granular rock. Journal of Structural Geology 28, 83–98.
Ben-Zion, Y., Sammis, C.G., 2003. Characterization of fault zones. Pure and Applied Geophysics 160, 677–715.
Bjørlykke, K., Høeg, K., 1997. Effects of burial diagenesis on stresses, compaction and fluid flow in sedimentary basins. Marine and Petroleum Geology 14, 267–276.
Brueckner, H.K., Snyder, W.S., Boudreau, M., 1987. Diagenetic controls on the structural evolution of siliceous sediments in the Golconda allochthon, Nevada, U.S.A. Journal of Structural Geology 9, 403–417.
Crider, J.G., Peacock, D.C.P., 2004. Initiation of brittle faults in the upper crust: a review of field observations. Journal of Structural Geology 26, 691–707.
Dehandschutter, B., Vandycke, S., Sintubin, M., Vandenberghe, N., Gaviglio, P., Sizun, J.-P., Wouters, L., 2004. Microfabric of fractured Boom Clay at depth: a case study of brittle–ductile transitional clay behaviour. Applied Clay Science 26, 389–401.
Dehandschutter, B., Vandycke, S., Sintubin, M., Vandenberghe, N., Wouters, L., 2005. Brittle fractures and ductile shear bands in argillaceous sediments: inferences from Oligocene Boom Clay (Belgium). Journal of Structural Geology 27, 1095–1112.
Eichhubl, P., Davatzes, N.C., Becker, S.P., 2009. Structural and diagenetic control of fluid migration and cementation along the Moab fault, Utah. American Association of Petroleum Geologist Bulletin 93, 653–681.
Engelder, T., Lash, G.G., Uzcátegui, R.S., 2009. Joint sets that enhance production from Middle and Upper Devonian gas shales of the Appalachian Basin. American Association of Petroleum Geologist Bulletin 93, 857–889.
Fossen, H., Schultz, R.A., Shipton, Z.K., Mair, K., 2007. Deformation bands in sandstone: a review. Journal of the Geological Society 164, 755–769.
Fossen, H., 2010. Deformation bands formed during soft-sediment deformation: observations from SE Utah. Marine and Petroleum Geology 27, 215–222.
Gross, M.R., 1995. Fracture partitioning: failure mode as a function of lithology in the Monterey Formation of coastal California. Geological Society of America Bulletin 107, 779–792.
Guiton, M.L.E., Leroy, Y.M., Sassi, W., 2003a. Activation of diffuse discontinuities and folding of sedimentary layers. Journal of Geophysical Research 108 (B4), 2183. doi:10.1029/2002JB001770.
Guiton, M.L.E., Sassi, W., Leroy, Y.M., Gauthier, B.D.M., 2003b. Mechanical constraints on the chronology of fracture activation in folded Devonian sandstone of the western Moroccan Anti-Atlas. Journal of Structural Geology 25, 1317–1330.
Hennings, P.H., Olson, J.E., Thompson, L.B., 2000. Combining outcrop data and three-dimensional structural models to characterize fractured reservoirs: an example from Wyoming. American Association of Petroleum Geologist Bulletin 84, 830–849.
Hiraga, N., Ishii, E., 2008. Mineral and Chemical Composition of Rock Core and Surface Gas Composition in Horonobe Underground Research Laboratory Project (Phase 1). Japan Atomic Energy Agency, Tokai-mura, Japan. JAEA Technical Report JAEA-Data/Code 2007-022.
Iijima, A., Tada, R., 1981. Silica diagenesis of Neogene diatomaceous and volcaniclastic sediments in northern Japan. Sedimentology 28, 185–200.
Ikeda, Y., 2002. The origin and mechanism of active folding in Japan. Active Fault Research 22, 67–70.
Ingram, G.M., Urai, J.L., 1999. Top-seal leakage through faults and fractures: the role of mudrock properties. In: Aplin, A.C., Fleet, A.J., Macquaker, J.H.S. (Eds.), Muds and Mudstones: Physical and Fluid Flow Properties. Geological Society Special Publications, vol. 158, pp. 125–135. London.
Ishii, E., Fukushima, T., 2006. A case study of analysis of faults in Neogene siliceous rocks. Journal of the Japan Society of Engineering Geology 47, 280–291.
Ishii, E., Yasue, K., Tanaka, T., Tsukuwi, R., Matsuo, K., Sugiyama, K., Matsuo, S., 2006. Three-dimensional distribution and hydrogeological properties of the Omagari Fault in the Horonobe area, northern Hokkaido, Japan. The Journal of the Geological Society of Japan 112, 301–314.
Ishii, E., Yasue, K., Ohira, H., Furusawa, A., Hasegawa, T., Nakagawa, M., 2008. Inception of anticline growth near the Omagari Fault, northern Hokkaido, Japan. The Journal of the Geological Society of Japan 114, 286–299.
Ishii, E., Funaki, H., Tokiwa, T., Ota, K., 2010. Relationship between fault growth mechanism and permeability variations with depth of siliceous mudstones in northern Hokkaido, Japan. Journal of Structural Geology 32, 1792–1805.
Ishii, E., Sanada, H., Funaki, H., Sugita, Y., Kurikami, H., 2011a. The relationships among brittleness, deformation behavior, and transport properties in mudstones: an example from the Horonobe Underground Research Laboratory, Japan. Journal of Geophysical Research 116, B09206. doi:10.1029/2011JB008279.
Ishii, E., Sanada, H., Iwatsuki, T., Sugita, Y., Kurikami, H., 2011b. Mechanical strength of the transition zone at the boundary between opal-A and opal-CT zones in siliceous rocks. Engineering Geology 122, 215–221.

Iwatsuki, T., Ishii, E., Niizato, T., 2009. Scenario development of long-tern evolution for deep hydrochemical conditions in Horonobe area, Hokkaido, Japan. Journal of Geography 118, 700–716.

Kai, K., Maekawa, K., 2009. Oxygen and hydrogen isotopic ratios and Cl^- concentration of saline water in the Neogene siliceous sediments of Horonobe, Hokkaido, Japan. Journal of the Japanese Association of Petroleum Technologists 74, 96–106.

Mazurek, M., Eggenberger, U., 2005. Mineralogical Analysis of Core Samples from the Horonobe Area. Institute of Geological Sciences, University of Bern, Switzerland. RWI Technical Report 05–01.

Mazurek, M., Gautschi, A., Marschall, P., Vigneron, G., Lebon, P., Delay, J., 2008. Transferability of geoscientific information from various sources (study sites, underground rock laboratories, natural analogues) to support safety cases for radioactive waste repositories in argillaceous formations. Physics and Chemistry of the Earth 33, S95–S105.

Mazurek, M., Alt-Epping, P., Bath, A., Gimmi, T., Waber, H.N., Buschaert, S., De Canniere, P., De Craen, M., Gautschi, A., Savoye, S., Vinsot, A., Wemaere, I., Wouters, L., 2011. Natural tracer profiles across argillaceous formations. Applied Geochemistry 26, 1035–1064.

Mitsui, K., Taguchi, K., 1977. Silica mineral diagenesis in Neogene tertiary shales in the Tempoku district, Hokkaido, Japan. Journal of Sedimentary Petrology 47, 158–167.

Myers, R., Aydin, A., 2004. The evolution of faults formed by shearing across joint zones in sandstone. Journal of Structural Geology 26, 947–966.

Mynatt, I., Seyum, S., Pollard, D.D., 2009. Fracture initiation, development, and reactivation in folded sedimentary rocks at Raplee Ridge, UT. Journal of Structural Geology 31, 1100–1113.

Nygård, R., Gutierrez, M., Bratli, R.K., Høeg, K., 2006. Brittle–ductile transition, shear failure and leakage in shales and mudrocks. Marine and Petroleum Geology 23, 201–212.

Okubo, C.H., Schultz, R.A., 2006. Near-tip stress rotation and the development of deformation band stepover geometries in mode II. Geological Society of America Bulletin 118, 343–348.

Sanada, H., Niunoya, S., Matsui, H., Fujii, Y., 2009. Influences of sedimentary history on the mechanical properties and microscopic structure change of Horonobe siliceous rocks. Journal of the Mining and Materials Processing Institute of Japan 125, 521–529.

Schultz, R.A., Fossen, H., 2008. Terminology for structural discontinuities. American Association of Petroleum Geologist Bulletin 92, 853–867.

Schultz, R.A., Siddharthan, R., 2005. A general framework for the occurrence and faulting of deformation bands in porous granular rocks. Tectonophysics 411, 1–18.

Silliphant, L.J., Engelder, T., Gross, M.R., 2002. The state of stress in the limb of the Split Mountain anticline, Utah: constraints placed by transected joints. Journal of Structural Geology 24, 155–172.

Torabi, A., Berg, S.S., 2011. Scaling of fault attributes: a review. Marine and Petroleum Geology 28, 1444–1460.

Vannucchi, P., Maltman, A., Bettelli, G., Clennell, B., 2003. On the nature of scaly fabric and scaly clay. Journal of Structural Geology 25, 673–688.

Wei, D., Seno, T., 1998. Determination of the Amurian plate motion. In: Flower, M., Chung, S.L., Lo, C.H., Lee, T.Y. (Eds.), Mantle Dynamics and Plate Interactions in East Asia. Geodynamics Series, vol. 27. American Geophysical Union, Washington, D.C., USA, pp. 337–346.

Wilkins, S.J., Gross, M.R., Wacker, M., Eyal, Y., Engelder, T., 2001. Faulted joints: kinematics, displacement-length scaling relations and criteria for their identification. Journal of Structural Geology 23, 315–327.

Yamamoto, H., 1979. The geologic structure and the sedimentary basin off northern part of the Hokkaido Island. Journal of the Japanese Association of Petroleum Technologists 44, 260–267.

Zhao, G., Johnson, A.M., 1992. Sequence of deformations recorded in joints and faults, Arches National Park, Utah. Journal of Structural Geology 14, 225–236.